Analysis of Periodic Clock Errors in Synchrophasor Ambient Data

Chetan Mishra
Dominion Energy, Richmond, VA
chetan.mishra@dominionenergy.com

Luigi Vanfretti
Rensselaer Polytechnic Institute
Troy, NY
luigi.vanfretti@gmail.com

T.J Purcell, Robert Orndorff, Jaime De La Ree Jr., Kevin.D.Jones
Dominion Energy, Richmond, VA

***Abstract*— Synchrophasor data from real world power systems are exposed to numerous adverse cyber-and-physical conditions that can negatively impact its fitness for use in PMU applications. While the most significant impairments like GPS signal loss, instrument transformer failures, data drop-offs, etc., have been studied in the literature, it is challenging to address other more complex nuisances that impact data quality. This is the case of differences in how clock synchronization, time-disciplining and phasor estimation is performed by different PMU vendors, that while frequently disregarded, have important implications on the data's fitness for use in PMU applications. In particular, ambient data applications, which have increasingly become a focus for tracking grid performance indicators, are extremely sensitive to periodic clock errors. Using synchrophasor and waveform data from Dominion Energy's power system, this article gives an in-depth analysis of the substaintial effect of seemingly minor device clock errors on measurement signal content.**

***Index Terms*— Clock error, Spectral analysis, Bicoherence**

I. INTRODUCTION

The increased use of power electronic-based resources such as renewable energy, FACTS devices, and the continued increase in new types of loads such as data centers, has resulted in unprecedented dynamic performance challenges, particularly localized issues caused by wrongly tuned controllers. The lack of transparent, portable and inter-operable dynamic models makes it difficult for utilities to perform conventional model-based analysis, leaving measurements as the only source from where to derive actionable information. Because a typical power system mostly operates in ambient conditions characterized by small and persistent random perturbations [1], taking a proactive approach to device performance monitoring necessitates the1eveloppment of techniques capable of extracting and analyzing the underlying system's dynamic purely from measurement data [2], [3]. In this regard, frequency domain measurement analysis approaches [4] have proven to be effective, owing to the fact that ambient dynamic characteristics resemble that of a stochastic linear system.

Working with real-world ambient data is difficult since the signals' power content of relevant dynamics is far lower than what is observed during events (i.e. transients or large disturbances). As a result, even small discrepancies with the IEEE Std. for Synchrophasor Measurements for Power Systems (IEEE C37.118.1-2011) [5] can have a significant impact on the observed ambient response exposed by the data and, as a result, data-driven applications. For example, discrepancies in frequency estimation techniques inside PMUs from different suppliers [6] will largely impact inertia monitoring [7].

Concerns related to time stamp corruption are the most challenging to address. The IEEE C37.118 std defines a Total Vector Error (TVE) limit of 1%, which equates to a phase angle error of 0.5730 (degrees) or a time synchronization inaccuracy of 21.6 μs at 60 Hz or 31.8 μs at 50 Hz. The majority of the existing body of work focuses on detecting more conspicuous issues, such as GPS signal loss [8], and their effects on applications. A related but inconspicuous issue that arises in ambient applications, notably modal analysis, is the drift in time stamps supplied by the internal oscillator of PMUs between two consecutive GPS time stamps (once a second). Our prior work on this topic [9] focuses on detecting and correcting spectral spikes in phase angle at multiples of 1 Hz, appearing as sharp horizontal lines in Fig. 1. The resulting conjecture from our previous work was that the impact of these periodic clock errors was limited to such spectral spikes. However, recent wide area studies on synchrophasor data in Dominion Energy's system have revealed new intriguing phenomena.

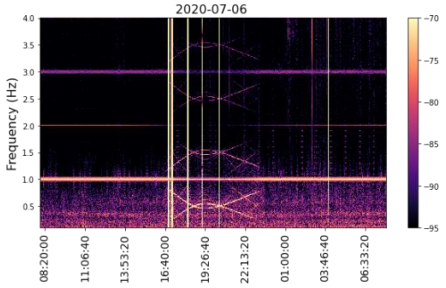

Fig. 1. Voltage Angle Derivative Spectrogram Showing Atypical Patterns

Figure 1 shows atypical symmetric patterns (17:00:00-23:00:00) of the phase angle dynamics in the time-frequency plane of a 500 kV nuclear power plant. These patterns will be

dissected herein, as they were eventually found to be pertinent to the aforementioned periodic clock errors, and thus, expanding the previously proposed conjecture.

This paper is organized as follows. Section II of this paper gives a brief background in signal processing techniques used in our work. Section III briefly describes the source of periodic clock errors as well as a theoretical analysis of the problem illustrated using both real measurements and synthetic signals. Finally, Section IV proposes an approach to distinguish periodic clock errors from actual power system dynamics by exploiting bicoherence.

II. Background

A. Power Spectral Density (PSD)

PSD describes how the signal's power is distributed over frequency. Letting $x(n)$ denote samples from a zero mean wide sense stationary (WSS) ergodic process, the autocorrelation function $r(k)$ is defined and estimated as,

$$r(k) = E(x(n)x(n+k))\ \forall k \in Z \tag{1}$$
$$\hat{r}(k) = \lim_{N\to\infty} \sum_{n=0}^{N-1} \frac{x(n)x(n+k)}{N}$$

where, $E(\cdot)$ is the expectation operator, the $\hat{}$ operator represents an estimate and N is the length of a sampled data window. PSD value $S(f)$ at frequency f, is then defined as,

$$S(f) = \sum_{k=-\infty}^{\infty} r(k)e^{-j2\pi fk}, |f| \le \frac{1}{2} \tag{2}$$
$$\hat{S}(f) = \lim_{N\to\infty} \frac{1}{N}|X(f)|^2$$

where $X(f) = \sum_{n=0}^{N-1} x(n)e^{-j2\pi fn}$. Here, we use Welch's method [4] to obtain a low variance estimate of $S(f)$. It works by dividing the data window into parcels and averaging spectrum estimates over them, sacrificing frequency resolution to reduce the estimate's variance.

B. Bispectrum and Bicoherence

Higher order moments are natural generalizations of the autocorrelation. For the above process, a general p^{th} order cumulant (second order is autocorrelation) is defined as,

$$c_p(k_1, \dots, k_{p-1}) = E(x(n)x(n+k_1)\dots x(n+k_{p-1})) \tag{3}$$
$$\hat{c_p} = \lim_{N\to\infty} \frac{1}{N} \sum_{n=0}^{N-1} x(n)x(n+k_1)\dots x(n+k_{p-1})$$

The Bispectrum [10], given in (4), is defined as the Fourier transform of the 3rd order cumulant and can yield insights into quadratic coupling between different frequency terms in the signal, usually resulting from nonlinearities.

$$B(f_1, f_2) = \sum_{l=-\infty}^{\infty} \sum_{k=-\infty}^{\infty} c_3(k,l)e^{-j2\pi(f_1k+f_2l)} \tag{4}$$
$$\hat{B}(f_1, f_2) = X(f_1)X(f_2)X^*(f_1+f_2)$$

Finally, bicoherence $b(f_1, f_2) \in [0,1]$, is a measure of phase coupling between frequencies f_1, f_2 and $f_1 + f_2$. In other words, it captures if $\angle X(f_1+f_2) - (\angle X(f_1) + \angle X(f_2))$ is constant and is defined as,

$$b^2(f_1, f_2) = \frac{|\hat{B}(f_1, f_2)|}{|X(f_1)X(f_2)|^2 |X(f_1+f_2)|^2} \tag{5}$$

Note that in the case of signals with finite length, the frequency domain of the bicoherence is bounded by Nyquist's frequency. As discussed in [11], bispectrum of the output $x(t)$ of a stable linear system driven by Gaussian inputs $u(t) \sim N(0,1)$ can be shown to be 0 as follows,

$$X(\omega) = G(\omega)U(\omega) \tag{6}$$
$$E(u(t)u(t+T_1)u(t+T_2)) = 0$$
$$\Rightarrow E(U(\omega_1)U(\omega_2)U^*(\omega_3)) = 0$$
$$\Rightarrow B(\omega_1, \omega_2) = E(X(\omega_1)X(\omega_2)X^*(\omega_1+\omega_2))$$
$$= G(\omega_1)G(\omega_2)G^*(\omega_1)E(U(\omega_1)U(\omega_2)U^*(\omega_1+\omega_2)) = 0$$

Here, $X(\omega)$ is the Fourier transform of $x(t)$ and $G(\omega)$ represents the transfer function of the system. Before proceeding, it is important to mention that ambient field measurements may violate the stationarity assumptions (in mean and spectrum) [1], which are required by the estimators in this section. This is a result of ever-changing operating conditions. That being said, operating conditions generally evolve over long time scales, resulting in a quasi-stationary spectrum with an approximately linear trend, which allows for using *long enough* windows (up to 30 mins) after simple detrending to obtain a sufficiently low variance spectral estimates for ambient data applications [12].

III. Clock Issues

A. Abnormal Observations in Real Measurements

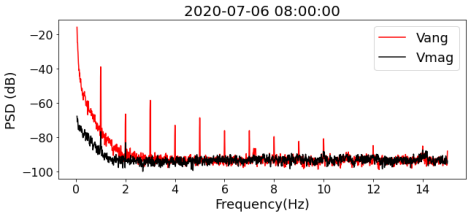

Fig. 2. Voltage Magnitude and Angle Spectrum

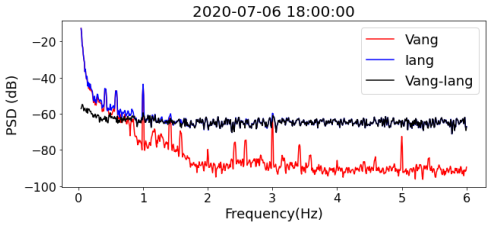

Fig. 3. PMU Voltage and Current Angle Spectra

To understand Fig. 1, we first start with a 10 min window at 08:00:00, a portion of the spectrogram with less "activity". The most prominent feature is exhibited by the voltage angle spectrum in Fig. 2, characterize by sharp peaks/spikes at 1 Hz and its multiples [9], which are barely visible in the voltage magnitude spectrum. Additionally, odd harmonics appear to be significantly more dominant than even harmonics, pointing to a symmetry between positive and negative cycles. Next, from Fig. 1, we analyze a 10 min window at 18:00:00, which appears to be significantly different, most likely due to operating changes in the power system around 17:00:00. Comparing the voltage and corresponding current phase angles reported by the same device, in Fig. 3, we see that a unique feature of these spectra are peaks around 0.4 Hz and

0.6 Hz. In addition, similar peaks are present at $k \times 1 \pm 0.4/0.6$_Hz. Finally, observe how these spikes are not visible in the angle difference, implying that the underlying mechanism behind these affects the V-I pair equally.

B. Effect of Clock Errors on Measurement Spectra

Let the "true" time be denoted by t and what the clock reports by τ, which is corrupted. For small errors, $\tau = t + \epsilon\phi_1(t)$ for some small ϵ. Here, $\phi_1(t)$ is a function arbitrarily normalized in $\in [-1,1]$. For small ϵ, an inverse function $\psi(\tau) = \tau + \epsilon\psi_1(\tau)$ exists that can recover the true time, t, from the corrupted one, τ. Now, if true system trajectory is $x(t)$, what is observed is $x(\psi(\tau))$, a perceived distortion. This is illustrated next.

Example 1: Let $x(t) = \cos(2\pi \times 0.2 \times t)$ and $\phi(t) = 2t \Rightarrow \psi(\tau) = \tau/2$. Here, the clock is significantly twice as fast as the true time t and therefore, the perceived dynamics appear slow, at half the frequency $x(\psi(\tau)) = \cos\left(2\pi\left(\frac{0.2}{2}\right)\tau\right)$.

To understand how differently the observed dynamics are from true dynamics, we obtain a Taylor expansion of the observed dynamics $x(\psi(\tau))$,

$$x(\psi(\tau)) = x(\tau) + \dot{x}(\tau) \times \epsilon\psi_1(\tau) + O(\epsilon^2). \quad (7)$$

Note that observed dynamics are comprised of $x(\tau)$, that is identical to the true system trajectory plus a term that multiplies its derivative to the clock errors $\epsilon\psi_1(\tau)$. This term is responsible for anomalies in the spectra seen in Fig. 3.

Next, we aim to understand the structure of $\psi_1(\tau)$ as it exists. The clock time stamps τ are generated by individual device oscillator, which is disciplined periodically (with a period T) using GPS time stamps (once a second) obtained from Global navigation satellite system (GNSS) station clock via IRIG-B signal. Thus, $t - \tau = \epsilon\psi(\tau)$ drops to 0 after ever T seconds (as fast as 1 second). Therefore, we can write it as a Fourier expansion $\psi_1(\tau) = \sum_k (a_k e^{jk\omega_0\tau} + a_k^* e^{-jk\omega_0\tau})\ \forall k \in Z^+$ where $\omega_0 = \frac{2\pi}{T}$ rad/s. These individual oscillatory components of the clock error will be referred to as clock modes herein. Substituting in the equation above,

$$x(\psi(\tau)) \approx x(\tau) + \epsilon\dot{x}(\tau) \times \sum_k (a_k e^{jk\omega_0\tau} + a_k^* e^{-jk\omega_0\tau}). \quad (8)$$

Because our analysis is in the frequency domain, obtaining the corresponding Fourier transform of (8) gives,

$$X_\psi(\omega) = (1 + \epsilon a_0 j\omega)X(\omega) + \epsilon \sum_{k>0} \begin{bmatrix} a_k j(\omega - k\omega_0)X(\omega - k\omega_0) \\ +a_k^* j(\omega + k\omega_0)X(\omega + k\omega_0) \end{bmatrix} \quad (9)$$

where $X(\omega)$ and $X_\psi(\omega)$ are Fourier transforms of $x(\tau)$ and $x(\psi(\tau))$ respectively. For the time being, assume that the true signal power $X(\omega)$ is concentrated at some ω_1 i.e. $|X(\omega \neq \omega_1)| = 0$. From (9), the apparent dynamics on the other hand will have non-zero power at $\omega_1 \pm k\omega_0 \forall k$ as well depending on $|a_k|$. Thus, periodic errors in clock creates new spectral components by interacting with actual system dynamics, which explains the symmetric spectral peaks to the left and right of 1 Hz, 2 Hz…(clock mode frequencies $k \times \omega_0/2\pi$) in Fig. 3. Another observation that can be made from (9) is that a_k, a component of a clock error can only be observed at ω through $|(\omega - k\omega_0)X(\omega - k\omega_0)|$, which is the amplitude of $\frac{dx(\tau)}{d\tau}$ at $(\omega - k\omega_0)$. Thus, a_k cannot appear at its corresponding frequency $k\omega_0$ unless, $\frac{dx}{d\tau}$ has a constant term (called a trend), in other words, $x(\tau) = b_0 \neq 0 + y(\tau)$. This is a bit of a surprise since both Fig. 2 and Fig. 3, that show real world data, have prominent peaks at $k\omega_0 = k2\pi\ \forall k$ but do not have trends. Before analyzing the source of trends, let us understand the effect of the magnitude of clock errors and the trend through two examples.

Example 2: Let the true measurement $x(t)$ be an output of a second order discrete time stochastic linear system model defined by $x(t) = \sum_{i=1:2} c_i x(t - i\Delta t) + b\varepsilon(t) \sim N(0,1)$ [4]. Here, $x(t)$ emulates typical ambient dynamics with a single arbitrarily placed mode at 0.2 Hz with a low 1% damping. Assume the clock error $\tau - t = \epsilon\phi_1(t) = \epsilon\frac{1+\cos(2\pi\times1\times t)}{2}$ with period $T = 1$ sec. Consider two different values of $\epsilon = 1 \times 10^{-1}$ and $\epsilon = 2 \times 10^{-1}$. The power spectral density of $x(\psi(\tau))$ in Fig. 4 shows that as the clock error becomes smaller, the error components a_k observed in the frequency domain also decrease. In addition, observe that while $\phi_1(t)$ has a single 1 Hz component, $\psi_1(\tau)$ also includes harmonics (see Fig. 5). Thus, $|a_k| \neq 0$ for $k > 1$ as well. These clock frequencies (0 Hz, 1 Hz, 2 Hz…) now interact with system dynamics characterized by the 0.2 Hz mode to yield components at $k \pm 0.2\ Hz\ \forall k$. However, because $x(t)$ has a fixed zero mean or no trend, we do not observe the clock modes at 1 Hz, 2Hz… themselves.

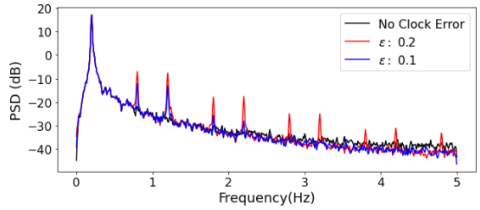

Fig. 4. Example 2, Corrupted (Synthetic) Signal Spectrum

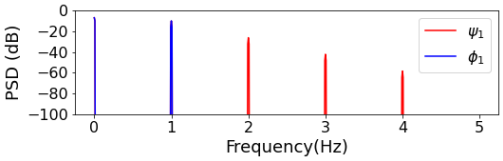

Fig. 5. Example 2, Periodic Clock Error

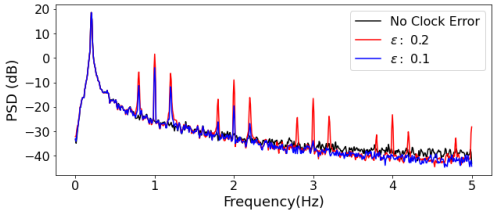

Fig. 6. Example 3, Corrupted (Synthetic) Signal with a Linear Trend

Example 3: Next, we demonstrate the effect of adding a trend to data. Let $x_{new}(t) = 2t + x(t) = \sum_{i=1:2} c_i x(t - i\Delta t) + b\varepsilon(t) \sim N(0,1)$. Before estimating the spectrum, $x_{new}(t)$ is detrended assuming a linear trend and the result is plotted in Fig. 6. A comparison of Fig. 6 with Fig. 4 demonstrates the role of trend in placing the effect of a_k at

$k\omega_0$ itself $\forall k$. Moreover, these spectral peaks grow with the increase in clock error. Here, it is important to mention that detrending cannot undo the effect of clock error.

C. Effect of Corruption at the Source (Waveform Data)

This section discusses how the stage at which the clock errors enter in the data pipeline has a major impact in the observed time (corrupted). It also clarifies the difference of the effect of clock errors on amplitude vs clock errors in the phase angle in PMU data and, finally, the source of trends in real world measurements.

To illustrate these issues, consider power system signals such as voltages and currents modeled in their purest form, waveform data, which is the input to a PMU's estimation algorithm. The power system dynamics observed by PMUs are modulated in both amplitude and phase of a carrier wave at frequency $f_c \approx 60\,Hz$ [2],

$$x_{wav}(t) = A(t)e^{j\theta(t)} \qquad (10)$$
$$\theta(t) = 2\pi f_c t + \rho(t)$$

where, $A(t)$ and $\theta(t)$ are the amplitude and phase of the waveform signal and $\rho(t)$ represents frequency dynamics. Now, synchrophasor estimates [13] reported by PMUs aim to capture $A(t)$ and $\rho(t) + 2\pi(f_c - 60)t$ from waveform data. It is now necessary to determine whether the clock errors corrupt the synchrophasor data directly or indirectly (if the waveform data is corrupted). For this, we plot the spectrum of the voltage waveform data previously analyzed window in Fig. 3 in Fig. 7. Any oscillatory components in $A(t)$ and/or $\theta(t)$ will appear as symmetric side bands of the carrier peak at $f_c \approx$60 Hz, corresponding to $f_c \pm kf_{mode}\ \forall k$ where f_{mode} is the oscillation frequency. Observe how the most prominent sidebands occur for $f_{mode} = 1$ Hz that as we know correspond to the clock modes. The same clock modes can be seen around the second (120 Hz) and higher harmonics of f_c. Thus, this confirms that the periodic clock error enters "upstream" (at the waveform stage), which results in corrupted phasors.

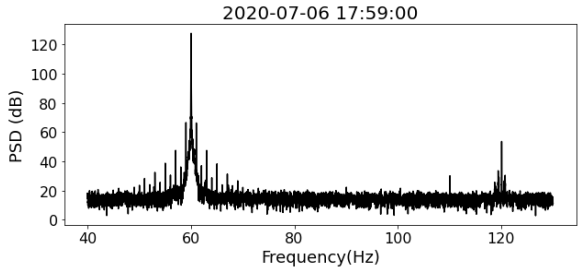

Fig. 7. Real-World Voltage Waveform Data Spectrum

To compare the relative level of impact on $A(t)$ vs $\theta(t)$, we need to understand how these signals, or rather their derivatives, typically behave as shown by (8). During ambient conditions, $A(t)$ moves in a narrow band around a constant operating point (e.g. 500 kV) and therefore, $\dot{A}(t)$ is extremely small in comparison to $A(t)$, resulting in an even smaller effect from the clock. On the other hand, $\dot{\theta}(t) = 2\pi f_c + \dot{\rho}(t)$ has a large term from the trend $2\pi f_c t$ resulting from the power systems operating at $\approx 60\,Hz$. Thus, $\theta(t)$ is closer to Example 3 while $A(t)$ is closer to Example 2 and consequently, the phase angles exhibit relatively larger spectral spikes, as confirmed by Fig. 2.

IV. Distinguishing from True System Dynamics

Having explained the mechanism behind clock errors distorting the observed dynamics and resulting in spurious modes in frequency domain, we now concentrate on how to discern them from true system dynamics. The approach proposed in this section exploits the fact that any form of spurious modes created from clock errors have a nonlinear coupling between them.

From (6), we know that a linear time invariant system driven by white noise (a good approximation to true ambient dynamics) has zero bispectrum. Corrupting those measurements with periodic clock errors still results in a zero bispectrum. This can be proved by substituting $X(\omega)$ from (6) in (9) to obtain $X_\psi(\omega)$. Because all the terms in $X_\psi(\omega)$ are of degree 1 in $U(\omega)$ and consequently, of degree 3 in the bispectrum estimate in (4), using $E(U(\omega_1)U(\omega_2)U(\omega_3)) = 0$ from (6) yields 0. On the other hand, the presence of a trend contributes to zero-degree terms in $U(\omega)$ in $X_\psi(\omega)$ and consequently some non-zero even degree terms in $U(\omega)$ the bispectrum expression, resulting in a non-zero value.

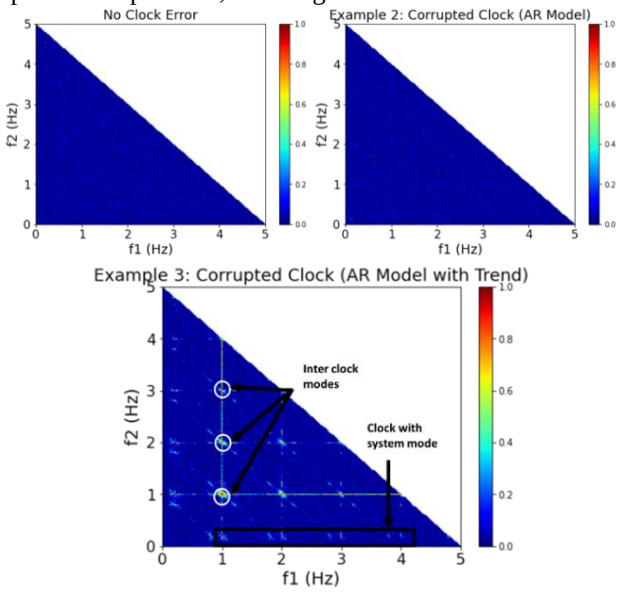

Fig. 8. Bicoherence of Clock-Corrupted (Synthetic) Signal with Linear Trend (Example 3) and without a Trend (Example 2)

This can be confirmed through bicoherence plots for data from Example 2 and Example 3 in Fig. 8. Focusing on Example 3's bicoherence plot, because the clock modes $a_k \forall k$ have fixed phases, there is a high bicoherence among the clock frequencies ($k \times 1$ Hz). Next high bicoherence is observed between clock mode frequencies and 0.2 Hz. Therefore, any spectral peaks at $(k \times 1) \pm 0.2$ Hz are deemed spurious. This also results in a high bicoherence between the clock modes and their created spurious modes.

Next, we offer a general guideline to distinguish between spurious clock-generated system modes and true system dynamic stability issues, manifested as poorly damped system modes. Note that automating such analyses for use in real-world applications is infeasible and generally requires human expert analyst. First, any kind of undamped oscillation, such

as clock error or true dynamics is characterized as narrow band peaks in PSD plot, which would warrant a deeper analysis. As discussed before, clock errors, would primarily be seen in phase angle, similar to angular electromechanical oscillations. These will occupy higher frequencies as well unlike poorly damped angular oscillations, that are usually < 1 Hz. This alone is not sufficient to distinguish between them owing to the influx of converter interfaced resources operating in a wide range of frequencies. Next we note that true modes do not interact with each other thereby resulting in 0 bicoherence. Therefore, if there is a sizable bicoherence between the frequencies of interest (possible undamped oscillations) and any other modal frequencies (that are not their harmonics), this is sufficient justification to categorize the problem as spurious in nature and clock related rather than related to system dynamic. Note that estimating the clock errors is necessary in order to "reverse" the effect of clock corruption, which will be explored in future.

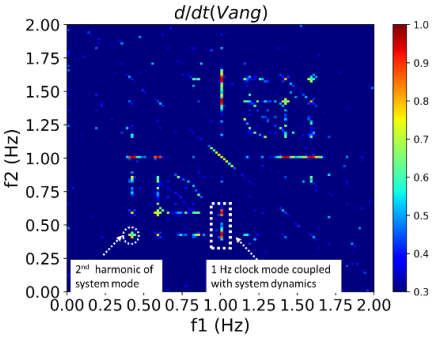

Fig. 9. Bicoherence for Fig. 3

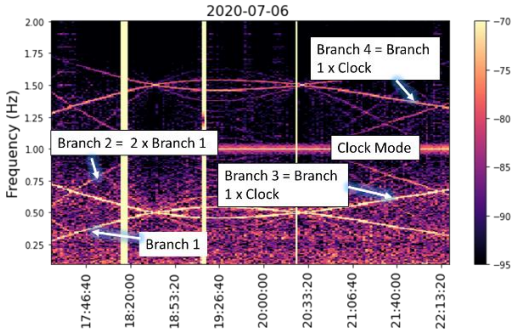

Fig. 10. Spectrogram Fig. 1 < 2 Hz

Finally, we perform bicoherence analysis on the real-world phase angle measurements corresponding to Fig. 1 and Fig. 3. The voltage phase angle data needs to be pre-processed. This is achieved by applying to it a derivative operation to remove the slow, non-stationary trend, while retaining the bicoherence values corresponding to ambient dynamics (derivative introduces a fixed phase shift). The bicoherence obtained is shown in Fig. 9. Next, the spectrogram of Fig. 1 is magnified for clarity and shown in Fig. 10. Starting from the lowest frequency, 0.4 Hz mode at 18:00:00 corresponds to Branch 1 in the spectrogram. It shows a high coupling with clock modes and also itself, which points towards a potential second harmonic [14]. From the spectrogram, one can see the second (harmonic) branch (labeled Branch 2) is at double the frequency and very similar in trajectory. Note that this the resulting peak around 0.8 Hz was not observed in the spectrum earlier (Fig. 3). Next, we can see the 1 Hz clock mode having strong coupling with 0.4 Hz, resulting in Branches 3 and 4 in the spectrogram at 0.6 and 1.4 Hz respectively around 18:00:00. The clock mode also shares a high bicoherence with these two branches as seen previously.

V. Discussion and Future Work

This work presents a detailed analysis of how periodic clock errors affect phasor measurements, particularly those of phase angles, to the extent that they are no longer fit for use' in ambient synchrophasor analytics. Bicoherence's ability to distinguish between clock modes and real system dynamics has also been demonstrated. Future research will explore estimating clock errors.

References

[1] A. R. Messina, *Inter-area Oscillations in Power Systems: A Nonlinear and Nonstationary Perspective*. Springer Science & Business Media, 2009.

[2] C. Wang, L. Vanfretti, C. Mishra, K. D. Jones, and R. M. Gardner, "Identifying Oscillations Injected by Inverter-Based Solar Energy Sources." arXiv, Feb. 23, 2022. doi: 10.48550/arXiv.2202.11579.

[3] C. Mishra *et al.*, "Analysis of STATCOM Oscillations using Ambient Synchrophasor Data in Dominion Energy," in *2022 IEEE Power & Energy Society Innovative Smart Grid Technologies Conference (ISGT)*, Apr. 2022, pp. 1–5. doi: 10.1109/ISGT50606.2022.9817489.

[4] P. Stoica and R. Moses, *Introduction to Spectral Analysis*, 1st edition. Upper Saddle River, N.J: Prentice Hall, 1997.

[5] "C37.118.1-2011 - IEEE Standard for Synchrophasor Measurements for Power Systems." https://standards.ieee.org/standard/C37_118_1-2011.html (accessed Oct. 03, 2020).

[6] C. Mishra, L. Vanfretti, K. Jones, and R. Gardner, *Designing Model-Free Time Derivatives in the Frequency Domain for Ambient PMU Data Applications*. 2022.

[7] C. Mishra, L. Vanfretti, and K. Jones, "Power System Frequency Domain Characteristics for Inertia Estimation from Ambient PMU Data," presented at the 2021 IEEE Power & Energy Society General Meeting, Jul. 2021. doi: 10.13140/RG.2.2.16404.63363.

[8] M. S. Almas, L. Vanfretti, R. S. Singh, and G. M. Jonsdottir, "Vulnerability of Synchrophasor-Based WAMPAC Applications' to Time Synchronization Spoofing," *IEEE Trans. Smart Grid*, vol. 9, no. 5, pp. 4601–4612, Sep. 2018, doi: 10.1109/TSG.2017.2665461.

[9] M. de Castro Fernandes, C. Mishra, L. Vanfretti, and K. Jones, "A Novel Method for Despiking Spectra from Synchrophasor Measurements," presented at the 2021 IEEE Power & Energy Society General Meeting, Jul. 2021.

[10] Y. C. Kim and E. J. Powers, "Digital Bispectral Analysis and Its Applications to Nonlinear Wave Interactions," *IEEE Trans. Plasma Sci.*, vol. 7, no. 2, pp. 120–131, Jun. 1979, doi: 10.1109/TPS.1979.4317207.

[11] M. Rosenblatt, "Linear Processes and Bispectra," *J. Appl. Probab.*, vol. 17, no. 1, pp. 265–270, 1980, doi: 10.2307/3212945.

[12] L. Vanfretti *et al.*, "Application of ambient analysis techniques for the estimation of electromechanical oscillations from measured PMU data in four different power systems," *Eur. Trans. Electr. Power*, vol. 21, no. 4, pp. 1640–1656, 2011, doi: 10.1002/etep.507.

[13] A. G. Phadke and J. S. Thorp, *Synchronized phasor measurements and their applications*, vol. 1. Springer, 2008.

[14] "Bicoherence analysis of nonstationary and nonlinear processes," *EUROfusion Scientific Publications*. https://scipub.euro-fusion.org/archives/eurofusion/bicoherence-analysis-of-nonstationary-and-nonlinear-processes (accessed Sep. 06, 2022).